Hindawi
International Journal of Optics
Volume 2023, Article ID 5538161, 18 pages
https://doi.org/10.1155/2023/5538161

Review Article

Classical and Quantum Surface Plasmon Resonance Biosensing

K. T. Mpofu,[1] **S. Ombinda-Lemboumba**,[1] **and P. Mthunzi-Kufa**[1,2,3]

[1]*Council for Scientific and Industrial Research (CSIR), National Laser Centre, Pretoria, South Africa*
[2]*School of Chemistry and Physics, University of KwaZulu-Natal, Durban 4041, South Africa*
[3]*Orthopaedic Biomechanics Lab, Division of Biomedical Engineering, Department of Human Biology, Faculty of Health Sciences, University of Cape Town, Anzio Road, Observatory, Cape Town, South Africa*

Correspondence should be addressed to K. T. Mpofu; kmpofu@csir.co.za and P. Mthunzi-Kufa; pmthunzikufa@csir.co.za

Received 12 June 2023; Revised 18 September 2023; Accepted 3 October 2023; Published 18 October 2023

Academic Editor: Yuan-Fong Chou Chau

Surface plasmon resonance is an optical phenomenon first discovered in 1902. The phenomenon has since had many applications, particularly in biosensing. In this paper, we review surface plasmon resonance-based biosensing, look at recent progress made in integrating quantum resources to develop surface plasmon resonance-based biosensors into a class of surface plasmon resonance biosensors commonly referred to as quantum surface plasmon resonance biosensors, and examine the advantages which quantum biosensors bring. We will review recent experimental and theoretical work showing that making use of quantum states of light offers a great enhancement in the precision of our biosensor, as they can go below the shot-noise limit (standard quantum limit) of precision in intensity noise detection. An overview of the surface plasmon resonance mechanism, its applications, and some limitations, as well as a report on recent research to address certain limitations and quantum-based surface plasmon resonance sensing, are provided.

1. Introduction

Over the past few decades, we have seen several new viral strains emerge around the world [1]. In the late 1990s, there was the HIV pandemic; then, in the early 2000s, that is, 2009-2010, we had the swine flu; in the recent 2000s (2014–2016), we have seen the Ebola outbreak; and most recently (2019), we had a COVID outbreak [2]. This is a very short list in a long list of outbreaks of diseases. Many are expected to occur over the next few years. One major problem is that viral strains are rapidly evolving, often faster than technology is capable of keeping up, leading to epidemics and pandemics. The occurrence of these disease outbreaks has heightened the importance of having precise diagnostics more than ever before, and optical biosensors, such as surface plasmon resonance (SPR)-based biosensors, are proving to be a strong contender in the fight against disease outbreaks [3–6]. SPR-based biosensors are not only good for providing accurate diagnostics but are also useful in drug development as well; rapid treatment development is also critical to stop the progression of associated diseases. SPR-based optical biosensors are reliable diagnostic devices that can make good point of care (PoC) systems due to their features such as portability, reproducibility, sensitivity, and specificity [7, 8]. SPR biosensors enable for the study of the binding kinetics of biochemical reactions that occur in a solution environment. In addition, they assess dissociation constants, binding and association rate constants, and stoichiometry for the kinetics of biochemical binding interactions. SPR is utilized for equilibrium analysis, concentration analysis, and kinetic analysis, all of which are crucial in detecting various phases of diseases like Epstein–Barr virus [9]. Identifying antibodies that bind to diverse antigens on a virus's surface can be utilized to determine the presence of specific illnesses [9]. SPR biosensors are an excellent tool for detecting the presence of these antigens. Beyond the realm of biosensing, SPR techniques also find utility in food monitoring [10], such as detecting antibiotics which are found exclusively in milk samples [11] and identifying the mycotoxin patulin [12]. SPR technologies have been used successfully in real time monitoring of the binding kinetics in a reaction between

dengue antibodies with its associated antigen [13]. The flexibility in terms of applications of SPR technologies and biosensors makes them very useful. SPR-based devices also have applications that include the detection and quantification of viruses such as the enterovirus 71 [14], membrane interaction studies which are applicable/applied to virus detection [15], and design of diseases such as COVID-19 [16]. SPR biosensors have surpassed traditional viral detection and quantification techniques in utility, and this is particularly true in the fields of medical diagnosis and healthcare [16]. A multibillion dollar global market exists for SPR-based biosensors, and major manufacturers include Biacore and Dynamic Biosensors.

In 1957, General Electric physicist Rufus Ritchie made a theoretical prediction of the existence of surface plasmons [17]. However, the SPR phenomenon had been observed earlier by Robert Wood, a physicist at Johns Hopkins University, in 1902. When Wood directed polarized light at a diffraction grating with a metal backing, he noticed a series of alternating dark and bright stripes in the light that was reflected [18]. This was the first recorded instance of SPR, but, at the time, there was no explanation for it. In 1907, Lord Rayleigh, a British physicist, was the first to develop a theoretical treatment of the optical observation of SPR in 1907. He hypothesized that the phenomenon was caused by the interaction between light and electrons on the surface of the metal. Dieter Otto demonstrated in 1968 that surface plasmon excitation arises as a result of attenuated total internal reflection (ATR), a technique that involves directing light at a particular angle through a prism or other transparent material to create an evanescent wave that interacts with the metal surface [19]. Otto Max Kretschmann and Heinz Friedrich Wilhelm Raether both obtained comparable results from a different ATR configuration in the same year (1968) [20, 21]. It was not until 1983 that Liedberg et al. demonstrated the application of SPR to biosensing [22]. Liedberg and colleagues showed that by coating a gold surface with a thin layer of biomolecules, they could use SPR to detect changes in the refractive index of the surrounding medium caused by the binding of complementary biomolecules. Since then, SPR technologies have developed into standard tools to study kinetic interactions between target molecules and biorecognition molecules. Surface plasmon resonance (SPR) became the core technology in affinity biosensors for the study of biomolecular interaction analysis (BIA) in the early 1990s [23]. These biosensors use SPR to detect and quantify the interactions between biomolecules, such as proteins and DNA, in real time and without the need for labeling or other modifications to the molecules. The fundamental/core principle of SPR-based BIA is to immobilize one of the biomolecules of interest on the sensor chip and then pass the other molecule over the surface. As the second molecule binds to the immobilized molecule, the refractive index at the surface changes, causing a shift in the SPR signal. By monitoring this shift, researchers can determine the strength of the interaction and other properties, such as the kinetics and affinity constants [23]. SPR technologies are prevalent to the point where they have been used to study diseases (and the viruses, organisms, or bacteria that cause them), such as AIDS (HIV) [24], COVID [25], and malaria [26]. It should be noted that there are other approaches regarding the properties and applications of plasmonic-based sensor structures which include MDM (metal-dielectric-metal) waveguide-based resonator [27–29], rod-shaped plasmonic sensor [30], and hybrid MDM-based plasmonic nanostructure [31, 32]. All of the simulations described in this work were generated using Mathematica code which was written by the authors. Any other programming language can be used for similar work such as Python and MATLAB.

Although SPR-based plasmonic nanosensors are commercially available, the precision of current SPR instrumentation is limited when it comes to measuring light reflectivity from the sensor. This limitation can lead to problems in various applications. For example, examining the movement and behavior of medications targeting various HIV-1 virus variants necessitates a level of accuracy beyond what is presently offered by commercially accessible SPR-based nanosensors [33]. In order to tackle this problem, scientists need to explore the underlying principles of the sensor's physics and take into account the foundational elements of optics, including resources rooted in quantum mechanics [34].

One very important parameter that is used to characterize the performance of a biosensor is its limit of detection (LoD). LoD is the minimal detectable change in a parameter of interest, x, where x can be the wavelength, refractive index, phase, or incident angle in the case of an SPR experiment. For a signal, y, the LoD of an SPR-based biosensor is dependent based on the transduction signal's measured noise, Δy, that is, the minimum resolvable signal.

$$\mathrm{LoD} = \frac{\Delta y}{S_y}, \tag{1}$$

where S_y is the sensitivity [26]. In order to improve the limit of detection (LoD) of SPR-based biosensors, researchers can either increase the sensitivity of the system or reduce the noise level. However, there are inherent limitations to how much the sensitivity can be improved due to the statistical nature of the light used in the system. The sensitivity of an SPR-based biosensor is determined by the magnitude of the change in the refractive index at the surface of the sensor, which is proportional to the amount of analyte bound to the sensor surface. The refractive index change causes a shift in the SPR signal, which can be measured with high precision using a detector. However, the precision of the detector is ultimately limited by the statistical fluctuations in the intensity of the light used to excite the plasmons at the surface of the sensor. This is known as shot noise, and it sets a fundamental limit to the sensitivity of the system [35]. According to research, the use of quantum states of light (such as the NOON, squeezed, and Fock) has great potential in reducing measurement noise, Δy, thus improves the LoD of plasmonic-based biosensors, going below the restrictive and classically limiting shot-noise limit (SNL) bound [35–40].

The formula for the sensitivity of the biosensor is given as follows:

$$S_y = \left|\frac{dy}{dp}\right|, \tag{2}$$

where p is a parameter to be estimated in the measurement of the signal y. The precision (LoD) with respect to the estimated p value is defined as follows:

$$\Delta p = \left|\frac{dy}{dp}\right|^{-1} \Delta y. \tag{3}$$

To compare the performance of various types of SPR sensors in detecting the refractive index, for example, we can rewrite the LoD formula with respect to the refractive index as follows:

$$\Delta n = \left|\frac{dy}{dn}\right|^{-1} \Delta y, \tag{4}$$

where n is the refractive index of the sample that the detector is monitoring. In general, for SPR biosensing, y can be either of the analysis quantities $(\lambda_{spr}, \Theta_{spr}, n_{spr}, \phi_{spr})$ where λ_{spr} is the wavelength of light incident on the biosensor, Θ_{spr} is the incident angle of light on the biosensor, n_{spr} is the index of refraction of the sample monitored by the biosensor, and ϕ_{spr} is the phase. The aim of this research is to reduce the noise in the transduction signal, Δy, which will lead to an improvement in the precision of the biosensor measurement, Δx. By applying quantum states of light, researchers hope to go beyond the limitations of classical metrology and achieve greater precision in biosensor measurements [34]. Quantum-enhanced SPR-based biosensors have already been shown to provide enhancement over their classical counterparts. In the later sections of the paper, we will discuss some quantum plasmonic resonance sensing and the potential of quantum biosensing to enhance the performance of SPR-based biosensors. This review provides an overview of the surface plasmon resonance mechanism, applications of SPR, and some limitations, as well as report on recent research to address certain limitations and quantum-based SPR sensing.

2. Introduction to Surface Plasmon Resonance

Surface plasmons are described or defined as collective oscillations of free electrons that occur at the interface between a metal and a dielectric material, such as air or water. These oscillations are evanescently confined to the interface, meaning that they decay exponentially in the direction perpendicular to the interface [41]. The ability of a metal to excite surface plasmons is determined by its electromagnetic properties, specifically its dielectric function or complex refractive index. Metals with a high density of free electrons, such as gold, silver, and copper, are often used for surface plasmon applications because they have a large negative real part of the dielectric function at optical frequencies, which allows for strong coupling between light and the collective oscillations of the electrons on the metal surface, known as surface plasmons. In contrast, metals with a low density of free electrons, such as aluminum and titanium, do not support surface plasmons at optical frequencies due to their weak coupling with light. Other factors, such as the size and shape of the metal nanostructures, can also affect the ability to excite surface plasmons. Gold or silver (for biological experiments, silver may not be used because of its antibacterial and antiviral properties) is typically used to excite surface plasmons because their electromagnetic properties (charge arrangement and conductivity) are the most suitable for getting an excitation response. Surface plasmon waves are evanescent waves whose propagation is confined to a metal-dielectric interface, as shown in Figure 1. The surface plasmon wave originates as a result of the coupling between an incident electromagnetic wave and oscillating electrons on a thin metal surface (at a specific angle of incidence of the electromagnetic wave). The conditions for this coupling to occur are discussed in the next section, where we derive the propagation coefficient. Figure 1 shows the excitation of surface plasmons by sending an electromagnetic wave towards a thin metal sheet through some dielectric medium of refractive index n_1. The surface plasmon is only few nanometers high. There are two main sets of configurations used to excite surface plasmons, called the Krestchmann configuration (Figure 1(a)) and the Ottoman configuration (Figure 1(b)) as shown in Figure 1. The difference being that, for the Krestchmann configuration, the analyte of interest sits on the surface of the gold and the plasmons are excited on the top part of the gold layer, while for the Otto configuration, the analyte of interest is between the gold layer and the prism and the plasmons are excited at the base of the gold. When SPR occurs, the intensity **R** (also known as reflectance) of the reflected electromagnetic wave is measured by the detector as shown in Figure 1 and decreases sharply (this happens as the angle of incidence of the incoming beam changes). The reflection coefficient or intensity (**R**) is determined by the angle of incidence of the incoming light and the refractive index of the analyte being examined. The reflection coefficient is defined as the ratio of the amplitude of the reflected wave to the amplitude of the incident wave [19]. The relationship between the reflection coefficient and the incident angle and refractive index can be described by Fresnel's equations, which are used in optics to calculate the reflection and transmission of electromagnetic waves at the interface between two media with different refractive indices. The minimum point of the intensity decline is sometimes referred to as an SPR dip, and this drop in energy is a result of the coupling of incident light with electrons in the metal layer. The profile generally resembles the plot in Figures 2(a) and 2(b), depending on whether the angle or index of refraction is changing. The intensity **R** of the electromagnetic wave reflected depends on the angle of incidence θ_i and the index of refraction of the dielectric medium sitting on the metal surface.

The resonance dip measurement can also be obtained from the change in the index of refraction, that is, by keeping the incident angle constant and changing the index of refraction of the dielectric on the biosensor surface (that is the metal surface), as shown in Figure 2(b). Changing the refractive index of the dielectric medium while keeping the

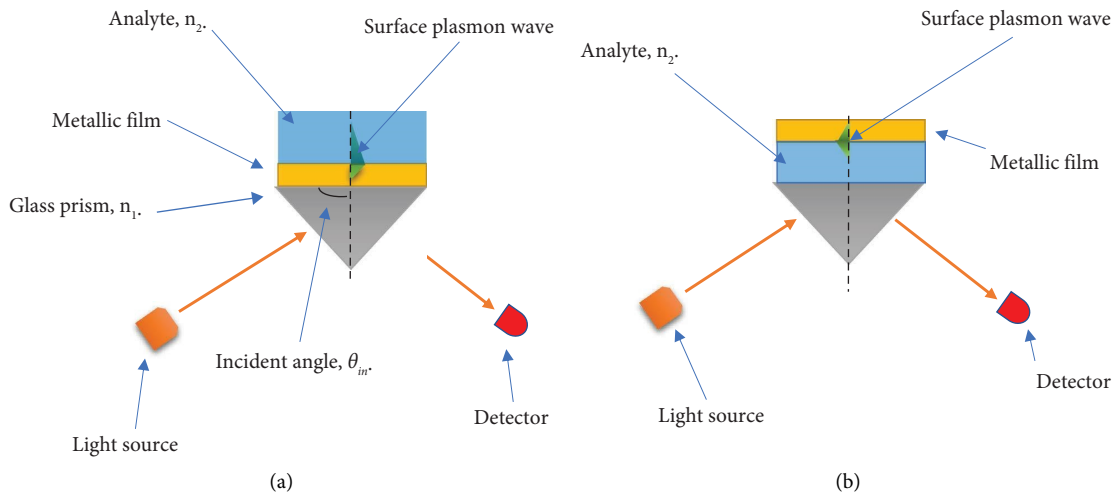

FIGURE 1: Exciting surface plasmons in prism configuration setups. (a) Krestchmann configuration setup and (b) Otto configuration setup. Figures (a) and (b) show how surface plasmons are generated in a prism-based SPR setup. There are two common configurations that can be used to excite surface plasmons, that is, the Krestchmann configuration shown in (a) and the Otto configuration shown in (b). Both configurations are practically useful, but the Krestchmann configuration tends to be easier to configure and is more commonly used. In these setups, light is sent at a varied angle of incidence towards a glass prism (BK7) that has a gold layer on its surface (or has a gold-coated slide sitting above it). This gold layer is only a few nanometers thick. At a certain angle, the incident light couples with oscillating electrons in the thin gold layer, resulting in an evanescent wave propagating on the gold surface, which is called the surface plasmon wave. When this surface plasmon wave forms, we observe a dip in the intensity of the reflected wave, which is collected by the detector. The surface plasmon wave is sensitive to changes in the dielectric properties of the analyte (with a refractive index n_2) on the surface of the gold. This sensitivity changing dielectric conditions on the surface of the gold is used for biosensing applications.

incident angle fixed above the resonance angle can be used to tune the SPR signal, and by altering the refractive index of the dielectric material, we can observe a decrease in the SPR signal, as shown in Figure 2(a). Because reflectance, **R**, is a collective function of both, angle of incidence and the index of refraction, we can study its relationship with either parameter by holding the other constant; however, we can construct the three-dimensional plot as shown in Figure 2(b). To find the angle of incidence and the index of refraction parameters that give the lowest resonance dip, Figure 2(c) shows a 3D plot of the dependence of **R**, both on the index of refraction and on the incident angle. This can be useful in identifying the true minimum of **R**.

3. Sensing Model

3.1. Propagation Coefficient Derivation from the Wave Vector. The dispersion relation is a mathematical expression that describes the relationship between the frequency and wavelength of a wave in a given medium. The propagation coefficient is vital for understanding the excitation of evanescent waves. It is the key result that tells us the conditions under which the coupling between the incident light and the metal plasmons can occur. In this section, we derive the propagation coefficient from the wave vector equation. To get a derivation of the propagation constant, it is critical to follow the calculation from the textbook of Maier [41]. To obtain classical field expressions for surface plasmons sustained by a single interface, Maxwell's equations are employed. Beginning with the wave equation, the dispersion relation in equation (5) can be obtained.

$$k_y = k_0 \sqrt{\frac{\epsilon(\omega)}{\epsilon(\omega)+1}}, \tag{5}$$

where k_0 is the free space permittivity of light, $\epsilon(\omega)$ is the dielectric function of the metal layer, and ω is a frequency.

3.2. Discussion of Sensing Techniques and Coupling Strategies. The propagation-dispersion relation is an important concept in the study of surface plasmon excitation. It describes the relationship between the momentum and frequency of the surface plasmon waves, which can be excited at the interface between a metal and a dielectric material. It also gives information on whether or not SPR can occur in a setup. Propagation relation studies for different media help us to understand the different combinations of materials that can excite surface plasmons. Figures 3(a) and 3(b) show the propagation relations in different media, and we can see the combination of media that allows the excitation of plasmon resonance.

From Figure 3(b), we can see that surface plasmons can only be excited at the metal-dielectric interface, where the mode matching condition is satisfied, that is, when $k_{\|SiO_2} = k_{\|sp}$. It is visible from Figure 3 that getting the coupling conditions is not an easy exercise in practice. It is also clear from Figure 3 that in the air-metal interface, the coupling conditions are never satisfied, that is, $k_{\|air} \neq k_{\|sp}$ meaning there cannot be any coupling without the introduction of some other medium. This is due to the fact that surface plasmon modes cannot directly interact with the far field (i.e., free space electromagnetic radiation) and vice

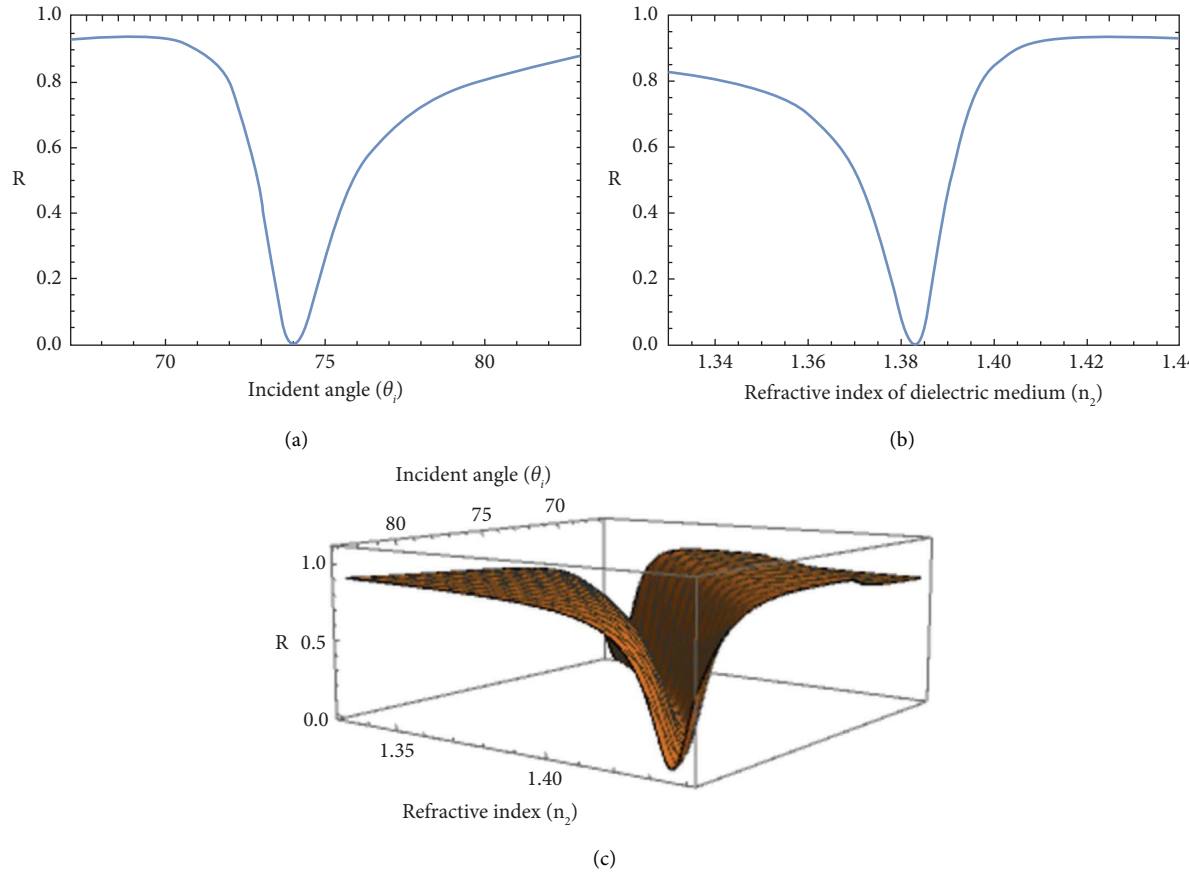

Figure 2: The dependence of the measured reflectance on the incident angle of light and the analyte's refractive index. As the angle of incidence of light hitting the prism changes, the intensity of the reflected beam R changes. This is because the incident beam begins to couple with the plasmons in the gold metal exciting them and generating a surface plasmon wave in the process; the energy of the beam is thus converted to this wave, and we start to get a drop in power. As the coupling becomes stronger and the evanescent waves become more intense, the reflected beam becomes weaker until it reaches the minimum point, that is, the resonance dip. (a) SPR dip with resonance angle. The same resonance dip effect can be observed when the incidence angle is kept constant and the refractive index changes instead. This is shown in (b) with an SPR dip plotted against the dielectric material's refractive index. (c) A 3D representation of the SPR dip is shown, considering the refractive index of the dielectric material and the angle of incidence. In this example, the coupling occurs at an incident angle of $\theta = 73^{\circ}$ and a dielectric material of refractive index $n_2 = 1.39$ and the refractive index of the prism $n_1 = 1.52$. This was taken from reference [40].

versa; this is known as the reciprocity theorem (which states that the coupling between two systems is the same, regardless of which one is the source and which one is the receiver). To solve this problem, we need to excite surface plasmons below the light line (i.e., at frequencies and wavevectors that are not accessible through conventional optical methods), and one common approach is to use a high refractive index medium, such as a BK7 prism or a grating, to couple light into the metal-dielectric interface at a specific angle of incidence. From Figure 3, light in the glass will not excite the plasmons bound at a metal/glass boundary, but they will be excited at the metal-dielectric interface if the mode matching condition is met, that is, where $k_{\parallel \mathrm{SiO}_2} = k_{\parallel \mathrm{sp}}$. From Figures 3(a) and 3(b), the mode matching conditions are satisfied at the crossing point between the dispersion curves.

There are many mechanisms reported to excite surface plasmons [43]. Here, we will briefly discuss four fundamental mechanisms for excitation of the surface plasmon, that is, through optic coupling, waveguide coupling, grating prism coupling, and fiber coupling. It also be noted that the SPR effect can also arise from SPR-based nanostructures [44–47]. This is due to a phenomenon known as localized surface plasmon resonance (LSPR) that occurs when metallic nanoparticles, typically gold or silver, interact with light [48, 49]. It is a type of SPR that happens on a nanometer scale, resulting in enhanced electromagnetic fields near the surface of the nanoparticles; however, this is not in the scope of this work. Prism couplers have been reported to be a convenient SPR configuration with a very small LoD; however, the size of the prism can be cumbersome and poses challenges in terms of incorporating it into other optical and electrical components [43]. There are a few strategies that can be used to mitigate these challenges. One approach is to use microprisms or nanoprism arrays, which can be much smaller than conventional prisms and can be fabricated using advanced lithography techniques. This can help to

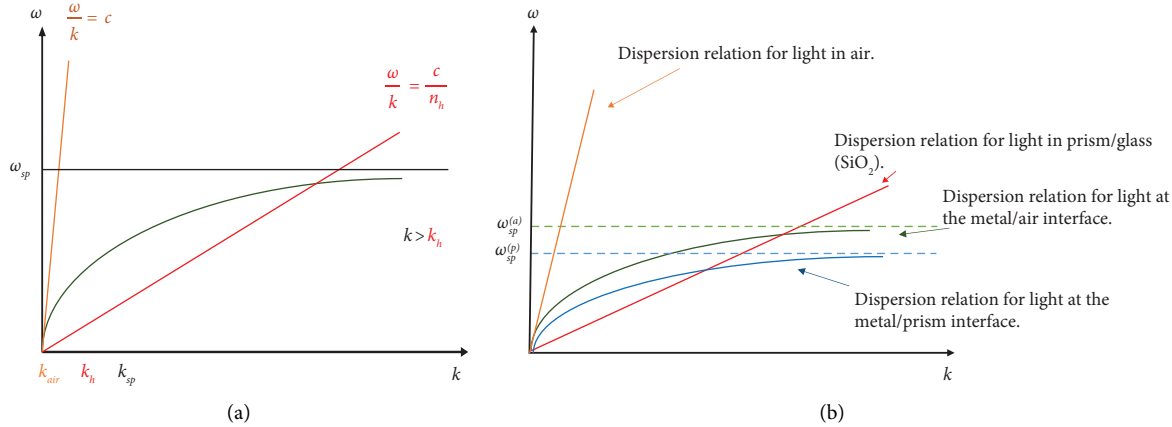

FIGURE 3: How the dispersion relation informs whether or not coupling can occur. (a) Diagram illustrating the propagation relationships in various media. ω is the surface plasmon frequency. The high-index medium is indicated by the letter "h" in the wave number k's subscript. This shows that if the electromagnetic wave does not propagate through some high refractive index medium first before hitting the gold layer in the setup, then there would be no coupling as the propagation coefficients never meet; however, if the light goes through some high-index medium, then there will be coupling. This figure was drawn from an example in reference [42]. (b) This graphic displays the propagation relations in a Kretschmann prism configuration as well as the reasons surface plasmons at the metal-glass contact cannot be activated (coupling conditions are not satisfied). If a prism (high refractive index medium, such as a BK7 SiO_2) is incorporated into the setup and the light passes through it first, surface plasmons are excited at the metal-air interface. This is demonstrated by the intersection of the blue prism dispersion line and the red surface plasmon dispersion curve at the metal/air contact. Surface plasmons at the metal/glass contact cannot be stimulated, according to the green curve. This figure was drawn from an example figure in reference [42].

reduce the overall size and complexity of the SPR setup. Waveguide coupling is also an alternative to the prism setup because the waveguide configuration has the advantage over the prism configuration that it is as robust and easier to incorporate with other electrical and optical components. Although the prism and waveguide mechanisms offer a low LoD, they have drawbacks that restrict their use. The inability of the evanescent field in SPR structures to permeate the surrounding medium beyond 100 nm makes it difficult to detect large target molecules. Examples of such molecules can be cells or bacteria, and this is one of these limitations [43]. Additionally, these mechanisms only have one surface plasmon for detecting changes in refractive index (RI). This makes it impossible to distinguish changes in the surface refractive index from bulk solution refractive index [50]. Some models have been proposed to minimize these disadvantages, that is, allow the sensor to differentiate the change in the background index of refraction and the surface-bound refractive change [7], and increase the penetration depth of the surface plasmon into the medium surrounding. Grating prism coupling is a versatile and efficient method for exciting surface plasmons on metal-dielectric interfaces [51–54]. This technique involves the use of a diffraction grating placed in contact with a metal surface, followed by coupling of light through a prism. The grating provides a periodic modulation of the refractive index, causing the incident light to couple into specific angles corresponding to the plasmon resonance conditions. This coupling mechanism is highly dependent on the grating parameters such as period, depth, and the refractive indices of the involved materials. By adjusting these parameters, researchers can control the excitation efficiency and the resonance angle of the surface plasmons. Grating prism coupling is particularly useful for studying localized and propagating surface plasmons and is commonly employed in various sensing and spectroscopy applications. Fiber coupling is another essential method for exciting surface plasmons, offering a flexible and remote approach [51, 55–58]. This technique involves the use of a tapered optical fiber that is brought into close proximity with a metal-dielectric interface. Light is launched into the fiber, and due to the strong evanescent field at the taper, energy is transferred to the surface plasmon modes. Fiber coupling is advantageous as it enables easy manipulation and positioning of the excitation point, allowing researchers to explore different regions of a sample [59]. Moreover, it offers compatibility with other optical components, facilitating integrated systems for sensing and imaging applications. However, it is important to consider the taper dimensions, polarization matching, and alignment precision to achieve efficient and controlled excitation.

Although four primary SPR sensing techniques exist, this paper will concentrate predominantly on the prism mechanism. The main reason being that the prism mechanism is a well-used mechanism, especially by companies such as Biacore, which manufacture biosensing devices, and it also easily translates into the quantum sensing regime [60]. The popular prism configuration is the Krestchmann configuration discussed previously (as opposed to the Otto configuration). In the prism mechanism, we can also study sensing submechanisms; for example, we can consider an intensity-sensing-based approach, a wavelength-sensing-based approach, an angular-sensing-based approach, and a phase-sensing-based approach in a prism-based approach such as the Kretschmann configuration. We will examine the intensity-based approach for this review because of the ease

with which it translates into the quantum sensing regime; however, in principle, we could also look at a phase-sensing approach [38]. The angular and wavelength-sensing approaches do not easily translate to the quantum regime but will be discussed briefly.

3.2.1. Angular Sensing. An angular interrogation SPR sensor measures the change in reflection intensity over a range of incident angles at a fixed wavelength (see Figure 4(a)) (λ, it is assumed that the wavelength of incident light here is fixed). The incident angle that corresponds to the resonance dip shown in the previous section is called the SPR dip angle and corresponds to the point where the coupling effect is strongest. The shift observed in the SPR resonance angle ($\Delta\theta$) corresponds to a change in the refractive index of the dielectric medium located on the gold surface (Δn_s). The relationship between the resonance dip angle to the SPR biosensor and the refractive index is shown in the following equation:

$$\theta_{\mathrm{SPR}} = \sin^{-1}\left(\frac{1}{n_p}\left[\frac{\epsilon_m(\lambda)\epsilon_{\mathrm{s}}}{\epsilon_m(\lambda)+\epsilon_{\mathrm{s}}}\right]^{1/2}\right), \tag{6}$$

where θ_{SPR} is the resonance angle of the SPR (the change in the resonance angle can be plotted as a time-dependent function, but this will be discussed when we look at interaction kinetics in the next section), λ is the wavelength of the electromagnetic wave incident on the prism, $\epsilon_m(\lambda)$ is the dielectric constant of the metal film, which is a function of the wavelength of the incident beam, λ, ϵ_s is the dielectric constant of the dielectric medium, and n_p is the index of refraction of the prism. Here, $\epsilon_s^{1/2} = n_s$, where n_s is the refractive index of the dielectric medium sitting on the surface of gold. When the index of refraction is fixed and the angle angle of resonance is changed, we obtain a drop in the resonance profile, as shown in Figure (2(a)). An interesting phenomenon occurs when the index of refraction of the analyte on the surface of the gold changes (this can be because of binding reactions on the prism surface), and the position of the dip shifts to the left or right, depending on whether the index of refraction value increases or decreases due to the dielectric medium on the surface of the metal plate. Figure 5 shows this change. In Figure 5, the index of refraction of the analyte on the surface of the prism changed from a value of 1.39 to 1.4, where the position of the dip changed to the right. In kinetic studies, researchers study this angle position drift (or reflectivity intensity drift) which is time dependent. As a result, we can obtain sensorgram plots that show dip angle drift over time. These drifts are essential in sensing experiments as they give information about binding parameters, such as binding constants, in kinetic binding studies. The sensitivity of the resonance angle to changes in nanoseconds (n_s) can be obtained from the coupling condition and can be written mathematically as follows:

$$S_\theta = \left|\frac{d\theta_{\mathrm{SPR}}}{\mathrm{d}n_s}\right|, \tag{7}$$

where

$$\left|\frac{d\theta_{\mathrm{SPR}}}{\mathrm{d}n_s}\right| = \frac{\epsilon_m(-\epsilon_m)^{1/2}}{\epsilon_s+\epsilon_m}\frac{1}{\sqrt{n_p(\epsilon_s+\epsilon_m)-\epsilon_s\epsilon_m}}. \tag{8}$$

Given the aforementioned relationship, it is clear that the refractive indices of the dielectric (analyte), the prism material, and the metal all affect the change in resonance angle. In principle, one could plot the sensitivity equation for different metals for comparison.

3.2.2. Wavelength Sensing. A wavelength-based SPR sensor measures the change in reflection intensity over a range of wavelengths at a fixed incident angle. Typically, with this biosensor, a broadband light source covers the target spectral range. Utilizing a spectrometer, the SPR spectrum is recorded. Here, a specific wavelength can also induce a SPR dip; this is the dip wavelength λ_{SPR}. The reflectance curve can also be calculated by measuring the incident light as a function of wavelength (or frequency) that is injected into the prism setup with a fixed incidence angle. The sensitivity to refractive index changes would be calculated as $|\mathrm{d}\lambda/\mathrm{d}n|$. Sensitivity can also be calculated as a function of wavelength, as shown in the following equation:

$$S_\lambda = \left|\frac{d\lambda_{\mathrm{SPR}}}{\mathrm{d}n}\right|, \tag{9}$$

where

$$\left|\frac{d\lambda_{\mathrm{SPR}}}{\mathrm{d}n}\right| = \frac{1}{{n_s}^3/2\left|d\epsilon_m/d\lambda\right| + \left[\epsilon_m + n_s^2\right]\epsilon_m \mathrm{d}n_p/d\lambda\, n_s/n_p} \times \epsilon_m^2. \tag{10}$$

3.2.3. Intensity Sensing. When utilizing an intensity-based SPR sensor, the reflected intensity is measured at a set incident angle and wavelength. If the coupling conditions for light surface plasmon have been fulfilled, there is a reduction in the reflectivity of the SPR dip, known as ATR. This leads to a near zero drop in the measured reflectance. To demonstrate that incident light is converted to a surface plasmon mode, we can solve the Maxwell equations. We calculate the reflection coefficient using three-layer system equations, which is expressed mathematically as follows:

$$r_{\mathrm{sp}} = \frac{e^{i2k_{2z}d}r_{23}+r_{12}}{e^{i2k_{2z}d}r_{23}r_{12}+1}, \tag{11}$$

where

$$r_{\mathrm{lm}} = \frac{k_{\mathrm{lz}}/\epsilon_l - k_{\mathrm{mz}}/\epsilon_m}{k_{\mathrm{lz}}/\epsilon_l + k_{\mathrm{mz}}/\epsilon_m}. \tag{12}$$

Here, $l, m \in \{1, 2, 3\}$, $k_{\mathrm{lz}} = \sqrt{\epsilon_l k_0^2 + k_Y^2}$, and $k_Y^2 = \epsilon_l k_0^2 \sin^2\theta_{\mathrm{in}}$, $k_0 = \omega/c$. ϵ_l is the respective permittivity, and d is the thickness of the metal layer. Reflectance, **R**, is proportional to the squared reflectivity coefficient ($\mathbf{R} \propto |r_{\mathrm{sp}}|^2$). The sensitivity to changes in the refractive index would be calculated as follows:

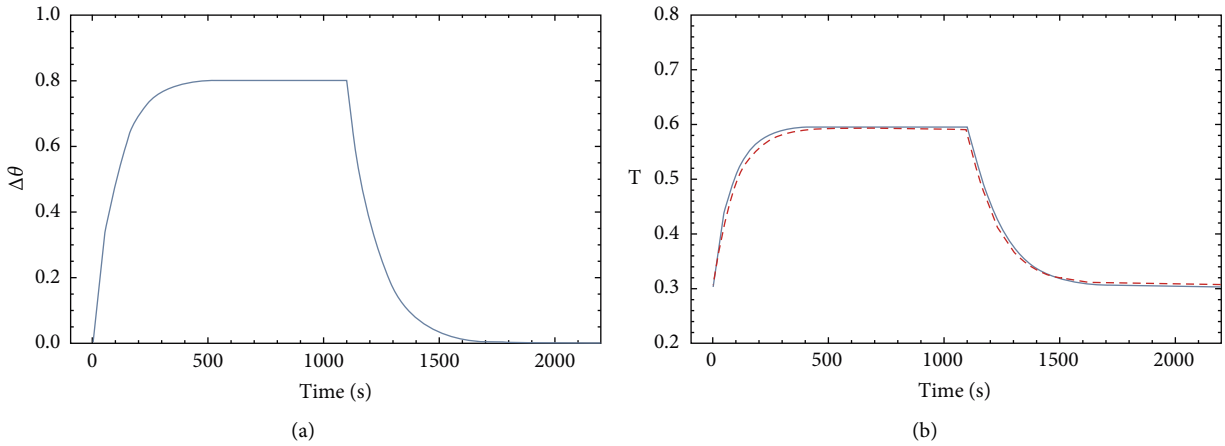

FIGURE 4: Angle-based and intensity-based sensorgrams generated from the work done by Kausaite et al. [5] investigating the interaction of bovine serum albumin (BSA) with rabbit anticow albumin antibody IgG1 (anti-BSA). In (a), there is angle-based (or angle-derived) sensorgram, $\Delta\theta(t)$, where the starting angle, $\theta(0) = 71.0966$ degrees. In (b), there is intensity-based (transmittance) sensorgram for the same binding reaction, $T(t)$ (solid line) and linearized reconstructed transmittance sensorgram, $T_L(t)$ (dashed line). For both transmittance sensorgrams, $\theta_{\text{in}} = 70.1200$ degrees have been set. The image was taken from reference [61].

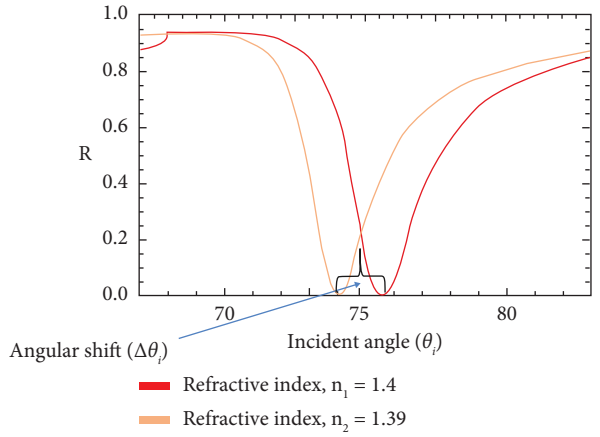

FIGURE 5: We see a shift/drift to the right in the position of the angle dip as the index of refraction of the analyte on the gold surface changes. The orange curve represents the curve obtained when the index of refraction of the analyte is 1.39 but as it changes to 1.4 a new curve is obtained, that is, the red curve is obtained and a new resonance dip position is established. The dip position is altered by changing the index of refraction of the dielectric on the gold surface. This shift is called the angular shift and corresponds to the change in refractive index. This figure was generated in Mathematica programming language using details from an example figure in reference [42].

$$S_R = \left|\frac{\mathrm{dR}}{\mathrm{d}n}\right|. \tag{13}$$

Here, **R** is the reflectance and S_R is the intensity sensitivity.

3.2.4. Phase Sensing. A phase-based SPR sensor measures the phase response with a change in angle of incidence and at a fixed wavelength. There is a steep slope of the phase response over a very small range of refractive index values. Phase modulation has previously been shown to give higher resolution compared to conventional SPR sensors based on angle and wavelength modulations [62]. From the Fresnel model [20, 21], the reflection coefficients of the p-polarization (which excites surface plasmons) can be expressed as follows:

$$r = |r|e^{i\phi}, \tag{14}$$

where r is the reflection coefficient described earlier and ϕ is the phase. Sensitivity to changes in the refractive index would be calculated as follows:

$$S_\theta = \left|\frac{d\phi}{\mathrm{d}n}\right|. \tag{15}$$

Here, θ is the phase and S_θ is the phase sensitivity.

3.3. Analysis of Binding Reaction Kinetics. Interaction kinetics describe the binding and unbinding processes between ligands and receptors, where receptors are described as chemical structures made up of proteins, and ligands are molecules that chemically bind to a receptor to create a biochemical complex. The interaction kinetics between the ligands and receptors is divided into three phases, namely, association, steady state, and dissociation. The three phases are shown in Figure 6. When a ligand binds to its receptor, the process is called association, and when equilibrium is reached and the quantity of binding and unbinding molecules is equal, the process is called steady state. Dissociation, on the other hand, refers to the process where the bonds between the complex molecules start to break or unbind more quickly than they can bind; [63] this can be because the ligands are being flushed out.

The complex concentration receptor ligand in the system at any time is mathematically written as $k_a[L][R]$. Here, k_a is a parameter called the association constant (which measures the rate at which a ligand and its receptor bind to form

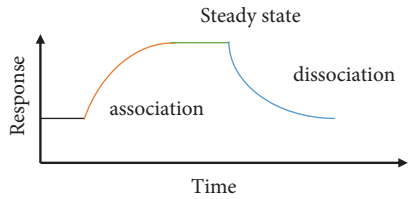

Figure 6: Three phases of interaction kinetics. The response unit may be related to a change in resonance angle, intensity, or refractive index, depending on what you are measuring. When the binding reaction begins, the signal change in the association region is observed (as receptor-ligand complexes form) up to the point where the binding surface is fully covered, at which point we observe a constant signal of the steady state; when we begin flushing out the ligand, we observe a sharp decline in the dissociation region, which is a result of rapid unbinding of the receptor-ligand complexes.

a complex) and is measured in per molar per second ($[M^{-1}s^{-1}]$). The collision rates between the ligand and the receptor molecules are used to determine the association constant. At time $t = 0$, the concentration of the receptor is expressed as $[R_0]$ and while the ligand concentration is expressed as $[L_0]$. Due to the employment of ligands and receptors, the concentration of receptor molecules decreases as the concentration of the receptor-ligand complex increases. At time $t \geq 0$, we have the concentration of ligands,

$$[L] = [L_0] - [C], \tag{16}$$

where $[C]$ is the complex concentration and the concentration of receptors,

$$[R] = [R_0] - [C]. \tag{17}$$

Reverse reactions in the equilibrium state can also be considered, where a decrease in the concentration of the receptor-ligand complex is directly proportional to an increase in the concentrations of the ligand and receptors. Here, the concentration of the ligand receptor is $[C]k_d$, where k_d is a parameter called the rate of dissociation constant and is measured in per second units ($[s^{-1}]$). Dissociation is a first-order reaction meaning the rate of dissociation is proportional to the concentration of the complex. In other words, as the concentration of the complex decreases, the rate of dissociation also decreases proportionally.

According to the law of mass action, the rate of a chemical reaction is proportional to the product of the concentrations of the reactants of the reactants raised to the power of the stoichiometric coefficients of the reactants. In the context of biomolecular interactions, this means that the rate of association or dissociation between a ligand and receptor is dependent on the concentration of both the ligand and receptor. At equilibrium, the rate of formation of the ligand complex should be equal to the rate of depletion of ligand and receptor concentrations, that is,

$$k_a [L][\dot{R}] = k_d [C]. \tag{18}$$

The ratio in equation (19) can be used to calculate the dissociation constant of the reaction,

$$\frac{k_d}{k_a} = k_D = \frac{[L][\dot{R}]}{[C]}. \tag{19}$$

The unit of the equilibrium dissociation constant is the molar. The reciprocal of the equilibrium dissociation constant, k_D, that is,

$$\frac{1}{k_D} = k_A, \tag{20}$$

k_A is a parameter called the affinity of the biochemical reaction. k_A is measured in unit per molar ($[M^{-1}]$). One can calculate the affinities of ligand-receptor interactions using a technique called equilibrium dialysis. This involves separating two solutions with a semipermeable membrane and waiting until the concentration of diffusible substances on both sides of the membrane, becomes equal. The equilibrium dialysis process is shown in Figure 7.

In Figure 7 the concentrations at time $t = 0$ of both ligands and receptors are $[R_0]$ and $[L_0]$, respectively, in the biosensor chamber. The complex concentration changes over time until equilibrium is reached, and this dynamic evolution is given by the equation,

$$\begin{aligned} \frac{d[C]}{\mathrm{dt}} &= k_a [R][L] - k_d [C] \\ &= k_a ([R_0] - [C])([L_0] - [C]) - k_d [C]. \end{aligned} \tag{21}$$

To solve the equation for the ligand-receptor reaction, the approximation of pseudo first-order reaction is utilized, as the reaction is a second-order reaction. This approximation assumes that the ligand concentration is in excess of the receptor concentration, denoted by $[L_0] \gg [R_0]$. Thus, the amount of ligand involved in the binding interactions is negligible relative to the ligand's initial concentration. This can be expressed as $[L_0] - [C] \approx [L_0]$, from which it follows that

$$\frac{d[C]}{\mathrm{dt}} = k_a ([R_0] - [C])([L_0]) - k_d [C]. \tag{22}$$

The pseudo first-order's solution, equation (22), equation is

$$[C] = \frac{[L_0][R_0]}{[L_0] + k_d/k_a} \left(1 - e^{(k_a [L_0] + k_d)t}\right). \tag{23}$$

When the reaction has reached equilibrium at time $t = \tau$, the concentration of complexes in the chamber increases to $[C_\tau]$. This is the point in time where the chamber is typically washed with a buffer, such as water, to remove any unbound ligand or receptor and to prevent any further binding from occurring. The decreasing rate of the complex is expressed as

$$\frac{d[C]}{\mathrm{dt}} = -k_d [C]. \tag{24}$$

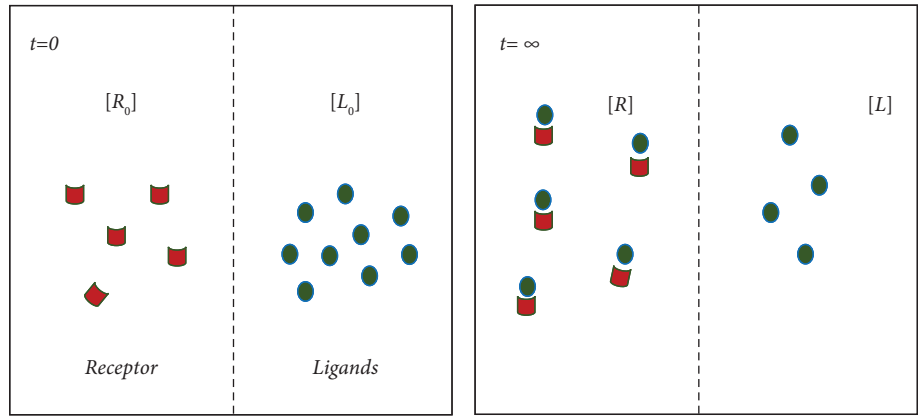

Figure 7: The schematic representation demonstrates the application of equilibrium dialysis for assessing the affinity between a ligand and receptor interaction, where a semipermeable membrane is portrayed by the dotted line at the center of a water chamber. The presumption is that the magnitudes of the association and dissociation rates are equal. The figure was drawn from a figure in reference [63].

As the buffer is introduced to the system, the concentration of the complex $[C]$ starts to decrease exponentially with time from the beginning of the elution process $t = \tau$. This is due to the fact that the concentration of the ligand $[L]$ decreases to zero with the introduction of the buffer. Figure 8 gives a picture of ligand-receptor interactions and how this can be mapped onto a sensorgram from which the binding kinetics can be extracted.

From Figure 8 when the buffer is pushed in, a resonance drop is observed, after which we let the analyte flow causing the resonance drop changes in intensity versus the SPR angle plot. This change can be tracked over time on a sensorgram, which measures the change in the SPR angle over time. Using the angle shift model (equation (25) below we can fit a model on the sensorgram from which we can get the binding parameters. When conducting experiments, the incident angle is typically fixed within a region around the SPR dip. The left side of the dip is the most sensitive region, and the change in reflectance is measured. The angular drift or shift $\Delta\theta$ or the reflectance/intensity drift or shift ΔR can be used interchangeably (i.e., you can go from the SPR angle change sensorgram to the intensity/transmission change sensorgram) in the sensorgram.

Following the calculations by Xiao [63], a mathematical model can be constructed that gives the sensorgram of the angle drift versus time. The mathematical model is used for theoretical biochemical reaction simulations which helps us understand the binding kinetics that occur (see the example in Figure 4(b), where they are investigating the interaction of bovine serum albumin (BSA) with rabbit anticow albumin antibody IgG1 (anti-BSA)). The model is as follows.

$$\Delta\theta = \begin{cases} A_{\infty}\left(1 - e^{-k_s t}\right), & 0 \le t < \tau, \\ A_{\tau} e^{-k_d (t-\tau)}, & t \ge \tau. \end{cases} \tag{25}$$

The change in resonance angle $(\Delta\theta)$ is a function of time (t), observable rate constant (k_s), and A_{∞} and A_{τ}, which are related to the sample concentrations. The rate constant (k_s) can be calculated as the sum of the product of the association constant (k_a) and the initial ligand concentration (L_0), and the dissociation constant (k_d), such that $k_s = k_a[L_0] + k_d$. By plotting $\Delta\theta$ against time, a sensorgram can be obtained, and the association and dissociation parameters can be extracted from it.

We can also study the kinetics of intensity-based sensorgrams (see the example in Figure 4(b), where they are investigating the interaction of BSA with rabbit anticow albumin antibody IgG1 (anti-BSA)). For the transmittance sensorgram (when there is a linear relationship between the concentration of the complex $[C]$ and the transmittance T), we can write [63]

$$T(t) = \begin{cases} T_{\infty}\left(1 - e^{-k_s t}\right), & 0 \le t < \tau, \\ T_{\tau} e^{-k_d (t-\tau)}, & t \ge \tau, \end{cases} \tag{26}$$

where T_{∞} is a constant (this constant is dependent on the initial receptor and ligand concentrations as well as the receptor and ligand thickness above the metal layer), k_A represents the affinity constant, the other constant, T_{τ}, depends on T_{∞}, and k_s is the association constant [61]. A rise in the complex concentration $[C]$ leads to an increase in the value of ϵ_a, which consequently increase T, when the angle of incidence of light remains constant.

3.4. Uses of SPR Kinetics. SPR is a method that can detect and quantify biomolecular interactions in real time without the need for labels. It can be used to study various types of interactions, such as interactions between biomolecules and nonbiological materials, interactions between proteins and proteins, interactions between DNA and DNA, and interactions between lipids and proteins. SPR enables the measurement of association and dissociation constants, known as k_a and k_d, respectively, which can be visualized on a sensorgram display. Analyzing biomolecular interactions with SPR has several benefits, such as identifying interactant binding, determining affinity, measuring k_a and k_d, and calculating the concentration of one of the interactants. The technique of SPR is employed for the analysis of interactions between biomolecules, and it offers valuable insights in

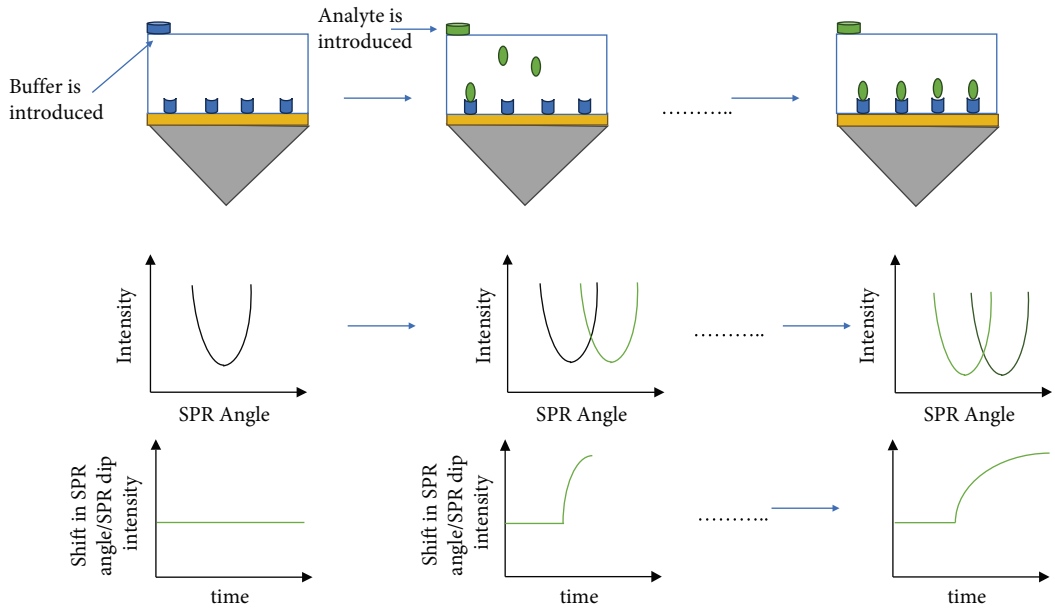

FIGURE 8: In the Krestchmann configuration setting, three phases of contact kinetics are generated from the angle shift. In the figure, after a buffer is passed through the biosensor, a resonance dip is observed at a particular angle, and the position of this dip shifts as the analyte is pushed through the biosensor. The SPR dip shift corresponds to a change in the index of refraction on the surface of the biosensor as binding reactions occur and can be plotted as a function of time. The change in the angle-dip position can be plotted as a function of time, resulting in the sensorgram below the intensity versus angle plots. If no analyte is passed through the biosensor, then there will be no change in the dip position, and hence the baseline remains constant. The change in the signal in the angle change versus time curve is due to binding reactions that occur as the analyte is introduced to the biosensor (this can be interpreted as a change in the concentration of the dielectric above the biosensor or a change in the index of refraction of the dielectric above the biosensor, both of which cause a signal change). The concentration of the complex $[C]$ and the response of the biosensor are linked by the index of refraction of the analyte $n_a = \sqrt{\epsilon_a}$ of the region above the gold surface, whose change is induced by the sequence of analytes passing through the flow cell: (i) buffer and ligands (association and steady state) and (ii) buffer only (dissociation). Figures were drawn from [33].

several ways: (1) detection of binding between the interacting molecules, (2) assessment of the strength of the interactions (affinity), (3) measurement of association and dissociation rates (ka and kd), and (4) estimation of the concentration of one of the molecules involved in the interaction. Kinetic parameters are useful for immunology studies, that is, in vaccine design and drug efficacy testing, and for diseases such as malaria, cancer, and Neisseria meningitidis [64].

4. Quantum Plasmonic Biosensing

This section will focus on intensity-based plasmonic sensing; this is because the intensity-based mechanism integrates easily with quantum resources. We examine how quantum optical resources can enhance the precision of SPR-based plasmonic biosensors. The quantum states discussed in this work are the two-mode squeezed displaced (TMSD), two-mode Fock state (TMF), two-mode coherent state (TMC), two-mode squeezed vacuum (TMSV), NOON, and two-mode product squeezed (TPS) states (see Figure 9). Despite the successful commercialization of SPR-based optical biosensors, they remain limited and restricted by the fundamental limit on the optical intensity noise (often observed in measurements with a photodiode or a CCD image sensor). This limit is a result of quantum fluctuations of light (related to the discreteness of photons) and is known as SNL. SPR-based biosensors such as those produced by Biacore use laser light to probe biological samples. Lasers produce coherent states of light whose intensity noise cannot go below the shot-noise limit (SNL). It is known that by using quantum states of light such as amplitude-squeezed light (generated by transforming coherent states via nonlinear interactions), we can get a noise below the SNL. The LoD of our biosensors is dependent on the noise of the signal measured in the biosensor; hence, by using quantum states of light, we can lower the LoD and the SNR ratio of our signal. In this section, we will look at the transition by using quantum states of light from recent SPR work. An example of a two-mode biosensing system is shown in Figure 10. A number of researchers have shown the enhancement that comes from using quantum states of light in SPR-based biosensing. Lee et al. in their paper [60] showed that two-mode quantum states of light that have symmetric statistical features in their photon number can improve intensity-sensitive SPR sensors. This work was followed by an analysis that looked at the TMSD state as a probe state in SPR biosensing where the authors showed an enhancement in the LoD when using this state [65]. In another paper [61], the authors studied the quantum-enhanced measurement of kinetic parameters in biochemical binding reactions using a range of different photonic quantum states and found that quantum states offer a great enhancement. The use of quantum states enables the detection of smaller

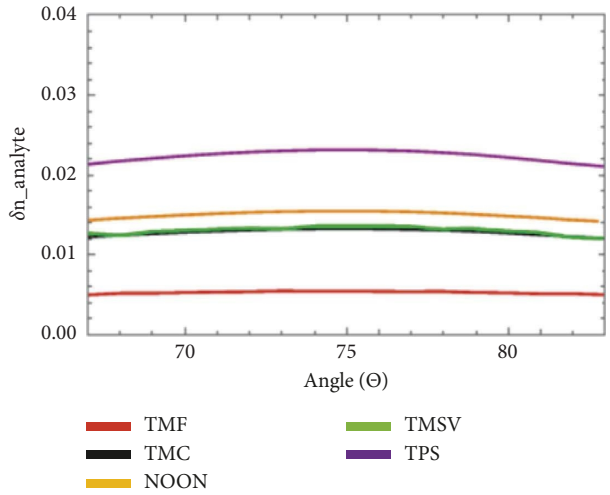

Figure 9: LoD for different quantum states with respect to the angle of incidence. The purple line is two-mode product squeezed state (TPS is a quantum state but does not give a good LoD for this experiment), the orange line is an entangled quantum state called the NOON state (it is not a good quantum state for this type of sensing but is good for phase-sensing experiments), the green line is two-mode squeezed vacuum state (TMSV is a quantum state which performs just as well as the coherent state for this type of sensing), the black line is the twin coherent state (TMC, in this case, is the baseline for the best classical state performance), and the red line is two-mode Fock state (TMF is a quantum state which has the best LoD in this case, and it far outperforms all the other states). It is clear that the Fock state gives the better enhancement since the LoD is the lowest; thus, we can see that quantum states can outperform classical states such as the coherent state, justifying the need for quantum biosensors to enhance precision in SPR-based biosensors. This was taken from reference [40].

concentrations of materials of interest in the same integration time or enables the detection of the same concentration of materials in a shorter integration time.

In this review, we look at new results from [39, 60, 61, 66] where the researchers consider a two-mode Krestchmann sensing model for SPR. The difference from a traditional single-mode model is that the two-mode setup has an extra path that has nothing done to it. Using this model, researchers showed the enhancement brought about by using quantum states of light in [39, 60, 61, 66]. The enhancement is in the LoD measurement of the refractive index, and for sensorgram measurements, they showed that quantum states of light can improve the precision of measured binding parameters. Due to their ability to overcome the limitations of conventional optical sensors in terms of sensitivity, flexibility, and photostability, SPR-based biosensors have become a powerful tool for biosensing applications [33, 67, 68]. Using quantum states of light can greatly improve these biosensors. As research continues to develop in SPR-based biosensors, different detection schemes are being developed which are being incorporated into a wide variety of biological and medical applications. Miniaturization and the improvement of precision measurements are some of the key driving forces behind research in plasmonic biosensors. A tool that can be used to address the miniaturization and development of PoC plasmonic-based devices is LSPR [33]. We will not discuss this here, as it is beyond the scope of the article.

Although SPR-based plasmonic nanosensors are commercially available, the precision of current SPR instrumentation is limited when it comes to measuring light reflectivity from the sensor. This limitation can lead to problems in various applications. For example, examining the movement and behavior of medications targeting various HIV-1 virus variants necessitates a level of accuracy beyond what is presently offered by commercially accessible SPR-based nanosensors [33]. In order to tackle this problem, scientists need to explore the underlying principles of the sensor's physics and take into account the foundational elements of optics, including resources rooted in quantum mechanics [34].

In [60], the LoD of the refractive index, Δn, is calculated for different quantum states using the following equation:

$$\Delta n = \frac{\langle \Delta \widehat{M} \rangle}{|d\langle \widehat{M} \rangle / \mathrm{d}n|}, \tag{27}$$

where $\widehat{M}$ is a measurement of the difference in the photon number between the two modes of interest, that is, the signal mode and the reference mode. The variance measurement $\langle \Delta \widehat{M} \rangle$ corresponds to the measurement noise in the model. $|\psi_{\mathrm{in}}\rangle$ is the input state in the sensing model. The lower the detection noise, the higher the precision (LoD) of our measured parameter; this is the refractive index, n, in this case. $|d\langle \widehat{M} \rangle / \mathrm{d}n|$ measures the sensitivity of the intensity difference to changes in the refractive index. $\widehat{M}$ is defined as follows:

$$\langle \widehat{M} \rangle = \langle \widehat{b}^{\dagger} \widehat{b} \rangle - \langle \widehat{a}^{\dagger} \widehat{a} \rangle. \tag{28}$$

Here, $\widehat{a}^{\dagger}\widehat{a}$ and $\widehat{b}^{\dagger}\widehat{b}$ are the photon number operators that count the number of photons of the states in mode a (signal) and in mode b (reference). According to Lee et al. [60], this reduces to

$$\langle \Delta \widehat{M} \rangle = \eta_b^2 \left(\langle \psi_{\mathrm{in}} \left| \widehat{b}_{\mathrm{in}}^{\dagger} \widehat{b}_{\mathrm{in}} \right| \psi_{\mathrm{in}} \rangle \right) - |r|^2 \eta_a^2 \left(\langle \psi_{\mathrm{in}} | \widehat{a}_{\mathrm{in}}^{\dagger} \widehat{a_{\mathrm{in}}} | \psi_{\mathrm{in}} \rangle \right). \tag{29}$$

Here, η_a and η_b are losses in modes a and b, respectively. The variance in intensity-difference measurement $\langle \Delta \widehat{M} \rangle$ is calculated as $\langle \Delta \widehat{M} \rangle = \sqrt{\langle \widehat{M}^2 \rangle - \langle \widehat{M} \rangle^2}$ which from Lee et al. reduces to

$$\langle \Delta \widehat{M} \rangle = N^{1/2} \Big[\left(\eta_b^2 - |r|^2 \eta_a^2 \right)^2 Q + 2|r|^2 \eta_a^2 \eta_b^2 \sigma + \eta_b^2 + |r|^2 \eta_a^2 \left(1 - 2\eta_b^2 \right) \Big]^{1/2}. \tag{30}$$

Here, the parameter Q is a parameter called the Mandel Q parameter and is different for different states of light (it measures the departure of the occupation number distribution from Poissonian statistics and can thus be used to differentiate between classical and quantum states of light) and σ is the noise reduction factor (NRF), which measures the noise reduction when different states of light are used.

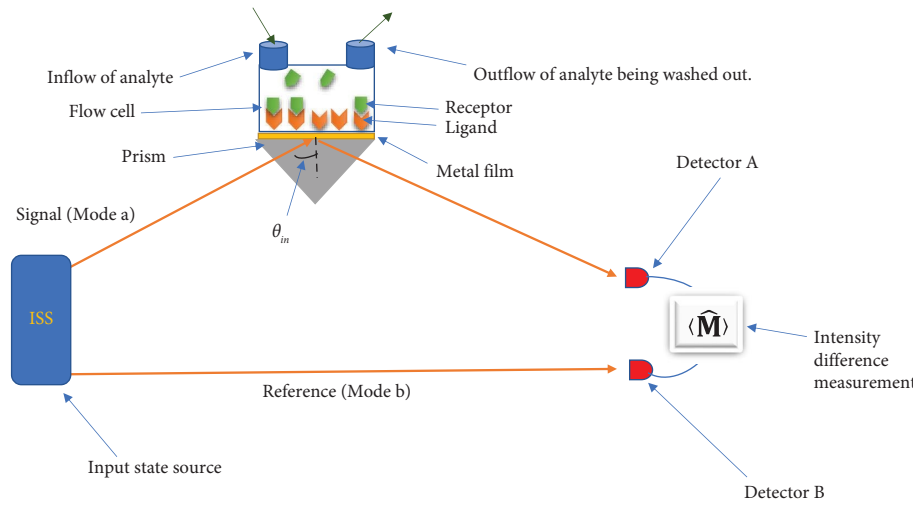

FIGURE 10: Two-mode biosensing setup. Model showing how a Krestchmann configuration setup can be integrated into a two-mode intensity-difference system. The signal mode goes to the prism and probes the system whereas the reference mode goes directly to the detector. The input states can be any state quantum or classical. Intensity-difference measurements have the added advantage of removing any background noise from the signal we are interested in. This was taken from reference [40].

There are many states of interest which we can compare to the coherent state, which we are taking as giving the best LoD achievable by a classical state (they are the minimum nonzero uncertainty states). As an example, when we consider the coherent and Fock states (calculations for these states and other states are shown in [60]), the $\langle \Delta \widehat{M} \rangle$ values are calculated as follows:

$$\langle \Delta \widehat{M} \rangle_{\text{Coherent}} = \left[|\alpha|^2 |r|^2 \eta_a^2 + |\alpha|^2 \eta_b^2 \right]^{1/2}, \tag{31}$$

for the coherent state and for the Fock state,

$$\langle \Delta \widehat{M} \rangle_{\text{Fock}} = N^{1/2} \left[-|r|^4 \eta_a^4 + |r|^2 \eta_a^2 - \eta_b^4 + \eta_b^2 \right]^{1/2}. \tag{32}$$

Comparing the intensity-difference variance measurements for the coherent and Fock states, the measurement noise in the Fock state will be significantly lower than that of the coherent state whose intensity noise is bound by the shot-noise limit (we look at the coherent state as the classical limit state, that is, the classical state that will have the lowest intensity noise), but here we will focus only on the Fock state because, for intensity-based sensing, it gives the best in LoD for refractive index measurements. Clearly, quantum states such as Fock states can provide a better LoD of the refractive index. A ratio R is calculated, and it compares the noise of the classical case with the quantum and measures the enhancement in precision brought about by using the quantum states. R is defined as $R = \langle \Delta \widehat{M} \rangle_{\text{Coherent}} / \langle \Delta \widehat{M} \rangle_{\text{Fock}}$. It follows that

$$R = \frac{\langle \Delta \widehat{M} \rangle_{\text{Coherent}}}{\langle \Delta \widehat{M} \rangle_{\text{Fock}}} = \frac{\left[|\alpha|^2 |r|^2 \eta_a^2 + |\alpha|^2 \eta_b^2 \right]^{1/2}}{N^{1/2} \left[-|r|^4 \eta_a^4 + |r|^2 \eta_a^2 - \eta_b^4 + \eta_b^2 \right]^{1/2}}, \tag{33}$$

$|\alpha|^2 = N$; hence, the above equation reduces to

$$R = \frac{\langle \Delta \widehat{M} \rangle_{\text{Coherent}}}{\langle \Delta \widehat{M} \rangle_{\text{Fock}}} = \frac{\left[|r|^2 \eta_a^2 + \eta_b^2 \right]^{1/2}}{\left[-|r|^4 \eta_a^4 + |r|^2 \eta_a^2 - \eta_b^4 + \eta_b^2 \right]^{1/2}}. \tag{34}$$

Setting $\eta_a = \eta_b = \eta$, we can reduce the expression even further and have

$$R = \frac{\langle \Delta \widehat{M} \rangle_{\text{Coherent}}}{\langle \Delta \widehat{M} \rangle_{\text{Fock}}} = \frac{\left[|r|^2 + 1 \right]^{1/2}}{\left[-|r|^4 \eta^2 + |r|^2 - \eta^2 + |r|^2 + 1 \right]^{1/2}}. \tag{35}$$

A plot of the ratio which measures the enhancement in noise reduction, R, is shown in Figure 11(a) for changing the resonance angle and in Figure 11(b) for changing the refractive index. In the region of the resonance dip angle and the resonance dip of the refractive index, the enhancement ratio, R, is maximized. The measured uncertainty of the Fock state becomes minimized compared to that of the coherent state, and from an experimental perspective, this would be the region where we would want to take measurements. Usually, in the Kretschmann setup, a laser serves as the light source, and within the quantum framework, laser light is aptly depicted as a coherent state [69]. Thus, we can begin to see the limitations of the currently available SPR-based biosensors. Limitations in the LoD of the refractive index can be overcome by studying the quantum nature of light.

Quantum states exhibiting non-Poissonian photon number distributions or nonclassical correlations have demonstrated the ability to surpass the SNL [70, 71]. In this section, we consider a result from a two-mode system in which the LoD, Δn, is considered for a particular experiment for different quantum states. We see that the LoD is a function of the incident angle and is dependent on the quantum state of the light used. By using Fock states of light, we can greatly improve the precision of our biosensor.

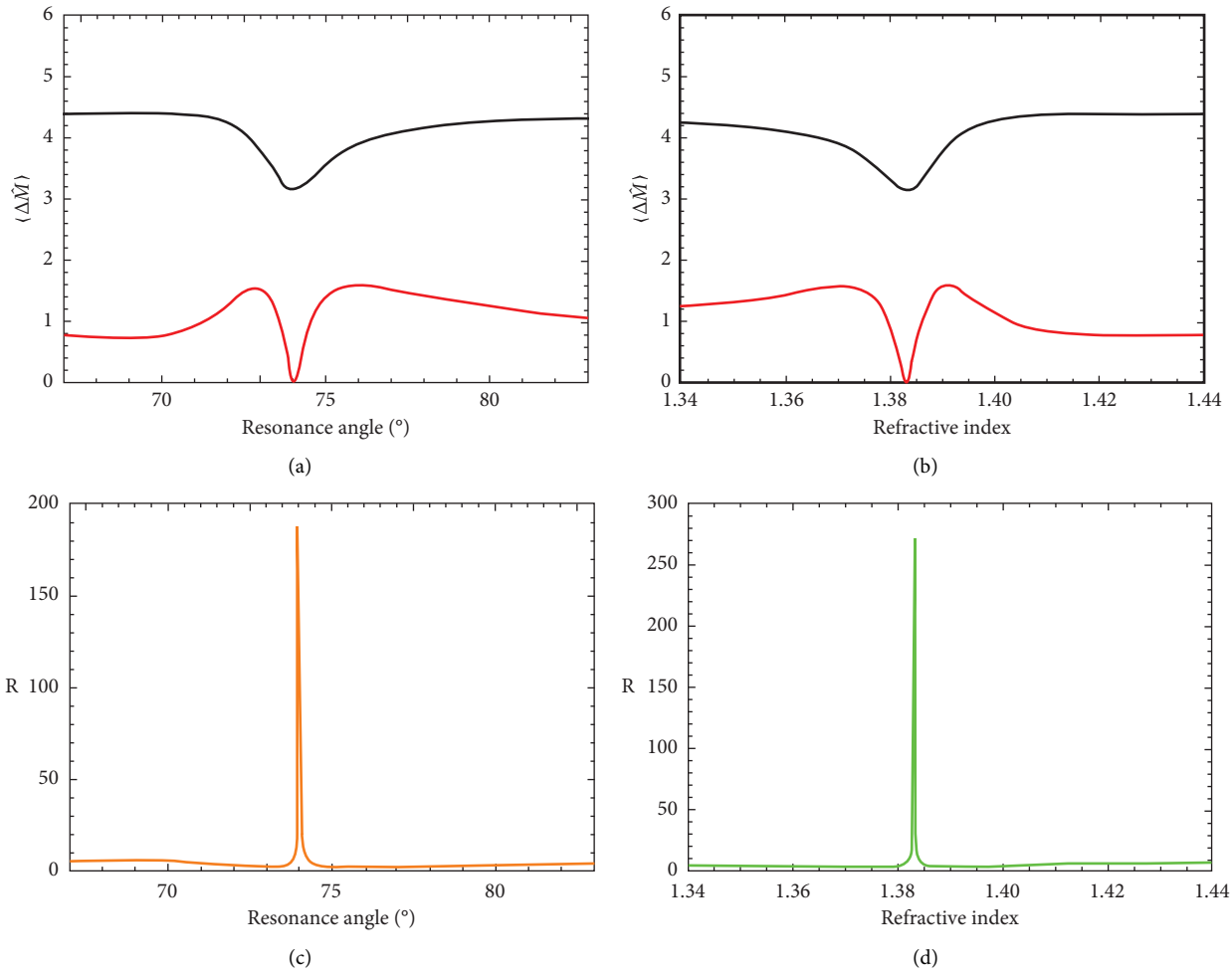

FIGURE 11: (a) A comparison of $\langle \Delta \widehat{M}_{\text{coherent}} \rangle$ with $\langle \Delta \widehat{M}_{\text{fock}} \rangle$. We see enhancement when Fock states are used versus the coherent state. (a) In this scenario, the resonance angle is fixed, and the analyte's refractive index is detected. The analyte has a refractive index of 1.39. (b) In this scenario, both the refractive index and the resonance angle of the analyte being sensed are set. Refractive index is 1.39, and the resonance angle is 73°. The coherent state is represented by the black line, and the Fock state by the red line. In the plot, it is assumed that there is no system loss in the setup, that is, $\eta_a = \eta_b = 1$. Photon number $N = |\alpha|^2 = 10$. (c) Enhancement ratio R. (d) Case in which the index of refraction of the analyte that is detected is fixed while the resonance angle is changed. The refractive index is 1.39 (b) in this scenario, the resonance angle of the analyte being sensed is fixed, and the index of refraction changes. The resonance angle is 73°. In the plots, it is assumed that there is no loss in the setup, that is, $\eta_a = \eta_b = 1$. Photon number, $N = |\alpha|^2 = 10$. This was taken from referecne [40].

Mpofu et al. [61] extend this work by looking at the enhancement in the precision of the measured kinetic parameters when quantum states are used. They considered a range of loss conditions when modeling the kinetics simulation but showed that Fock states consistently give better precision compared to the classical coherent states. It has also been shown experimentally that quantum states of light (single photons) give better precision in the measured kinetic parameters [60, 61].

5. SPR Experimental Setup

The goal of this section is to describe experimentally how an SPR experiment can be setup in the lab by proving an example and also briefly describing how a classical SPR setup can be converted into a quantum SPR source by integrating a single photon source as input to the setup (see Figures 12(a) and 12(b)). The paper by Pluchery et al. [72] is a great reference for experimentally setting up an SPR experiment. The SPR experiment using the Kretschmann configuration is a relatively simple experiment that can be easily conducted in a laboratory setting using optical components. From Figure 12(a) for the classical part, we see how different components can be arranged; an example laser source can be a 785 nm wavelength semiconductor diode unpolarized monochromatic 50 mW laser light source. To implement the quantum SPR experiment, this laser source will be replaced with a single photon source. A laser source can be used in conjunction with a microscope objective with a calibrated aperture, typically with a magnification of 20x, to function as a beam expander. The characteristics of the microscope objective cause the laser beam to grow and change into a collimated beam as a result. To increase the intensity of the beam coming from the microscope objective,

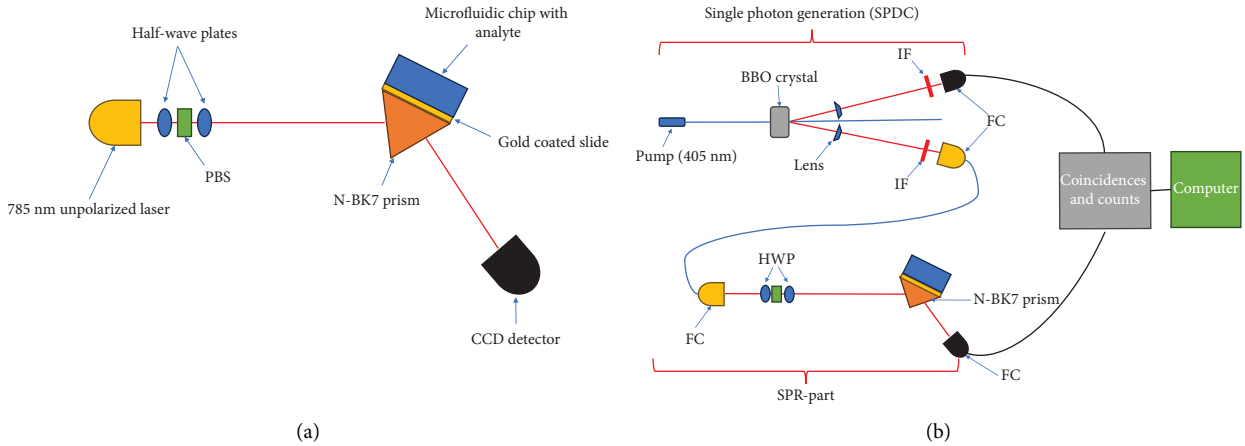

FIGURE 12: (a) An experimental setup used for SPR biosensing. Before striking the prism with the gold slide, a 785 nm unpolarized laser beam passes through two half-wave plates, a PBS, and then excites the surface plasmons at the metal-air interface. A CCD camera is used to capture the prism's reflected light. There is a flow cell on top of the gold layer that contains the analyte of interest. (b) A modified version of the SPR setup; it is modified in that the light source is no longer a laser but a single-photon source (SPDC source). This is an experimental example of single-photon plasmonic sensing from an SPDC source. In this case, the detectors will be single-photon detectors. The detectors measure coincidences and counts of single photons. This was taken from reference [40].

light is focused from the objective towards a half-wave plate. From the microscope objective, the light is directed towards a half-wave plate which is used to maximize the intensity of the beam from the objective. From the half-wave plate, the light is directed towards a polarizing beam splitter (PBS) that lets through the horizontally polarized component of the beam (p) and reflects out vertically polarized component of the beam (s). Another half-wave plate can be added after the PBS, which can be used to rotate the polarization between the s or p polarization; it is useful if the researcher is interested in investigating the s polarization.

From the second half-wave plate, the beam is guided towards a high-index equilateral prism (refractive index- = 1.601, for example). SPR glass slides (40 nm thick, gold-coated slides) are perched on the prism. In order to prevent an additional layer (air, for example, which would be a dielectric and introduce a variable refractive index) from being present between the surface of the prism and the gold slide, index-matching liquid is supplied. This keeps the refractive index approximately constant. Employing gold slides rather than applying a thin gold film on the prism surface offers multiple benefits. First, it enables the utilization of optimized gold thin films, since the film's thickness is crucial and governs the extent of coupling that takes place. Second, it facilitates the convenient substitution of the gold surface in case of damage. Rotation stages which are automated, for example, can be used to adjust the incident angle θ_{ext} (The mirrors and rotation angles are not shown in Figure 12(a)).

The beam reflects off the prism and is aimed towards a CCD detector that is connected to a computer for the classical case. For the quantum case, single-photon detectors are used, and intensity data are stored and processed on a computer system. Figures 12(a) and 12(b) which show the arrangement of components in the setup are known as the Kretschmann configuration, and the setup is shown in Figure 12(a). Over the range of angles where there is 100% internal reflection from the prism, surface plasmons are stimulated; hence, the critical angle of the setup needs to be identified during the calibration of the setup. It is important to note that in experiments, surface plasmons can only be excited in metal films that are thin enough (with the specific thickness determined by the type of metal used) and only with a specific polarization of light, known as the p-polarization.

5.1. Using SPDC Source for Single Photon Plasmonic Biosensing. In this section, we explore how quantum plasmonic sensing experiments can be carried out using quantum states of light in an SPR biosensing setup, achieved by merging the SPR and SPDC configurations, as shown in Figure 12. In [66], a single-photon-based proof-of-principle experiment is presented that uses quantum sensing techniques to improve the precision of the kinetic parameters (that is, an experiment with the configuration as shown in Figure 12(b)). In their study, the researchers examined the interplay between BSA binding to gold through an electrostatic process. They utilized single photons (created by parametric down-conversion) to investigate the BSA-gold interaction within a plasmonic resonance sensor. Researchers reported sub-shot-noise level fluctuations in the sensor signal that improved precision for values in the kinetic parameters, highlighting the potential use of quantum states of light for sensing in biochemical research. While a coherent beam with many photons might offer better noise reduction, the use of single photons is sufficient to demonstrate the relative enhancement offered by quantum plasmonic sensing. Additionally, the use of single photons can help avoid unwanted effects that might arise from the collective behavior of large numbers of photons [60]. In the quantum SPR experiment, Figure 12(b) coincidences and single counts of idler arms (top) and signal (bottom) were

measured and used in the analysis. Mpofu et al. [61] showed that an improvement in precision of up to 31.8% is possible in the values of the kinetic parameters. This can be attributed to the diminished noise associated with single-photon statistics, corroborating recent theoretical forecasts. The study demonstrates that employing quantum light sources for sensing kinetic parameters is a viable option, offering enhanced accuracy compared to traditional methods. Future work in this area could involve looking at sources such as the TMSD state and the TMSV state to enhance biosensing precision.

6. Conclusion and Outlook

In this paper, we review classical SPR-based biosensing and look at recent progress made in terms of the development of quantum SPR biosensors and the advantages that quantum biosensing brings. We reviewed fundamental details about SPR and looked at how to excite a surface plasmon as well as the conditions in which surface plasmons are excited. We looked at interaction kinetics and how they can be useful for biosensing and drug discovery applications, and we also detailed mathematical models for binding reactions. We compared classical SPR biosensing with quantum SPR-based biosensing and showed that using quantum states of light offers a great enhancement in the precision of our biosensor, as they are able to go below the SNL of intensity noise detection. We also looked at an experimental implementation of the SPR biosensor and a quantum experimental implementation that involved a single-photon source. Here, we see that quantum technologies are the next stage in enhancing biosensor performance, as they are already showing that they are capable of going beyond the SNL and facilitating a lower LoD for biosensing applications. Quantum biosensing offers great potential for better biosensing devices, and some of the information in this paper can offer a baseline from which to begin the application of quantum resources in biosensing. There is a lot of future work that can be carried out in both the classical and quantum areas of research. In the quantum space, researchers can begin to look at the two-mode squeeze displaced states and how they can be used for biosensing enhancement.

Abbreviations

SPR: Surface plasmon resonance
TMSD: Two-mode squeezed displaced
LoD: Limit of detection
RI: Refractive index
DNA: Deoxyribonucleic acid
CCD: Couple-charged device
SNL: Shot-noise limit
BSA: Bovine serum albumin
SPDC: Spontaneous parametric down-conversion
LSPR: Localized surface plasmon resonance
PoC: Point of care
TMSV: Two-mode squeezed vacuum
TPS: Two-mode product squeezed
TMF: Two-mode Fock
TMC: Two-mode coherent
MDM: Metal-dielectric-metal.

Data Availability

The data supporting the current study are available from the corresponding author upon request.

Conflicts of Interest

The authors declare that they have no conflicts of interest.

Acknowledgments

The authors acknowledge the Council for Scientific and Industrial Research (CSIR) and the Department of Science and Innovation (DSI) for funding granted for this research.

References

[1] D. T. Jamison, "Disease Control Priorities, 3rd edition: improving health and reducing poverty," *The Lancet*, vol. 391, no. 10125, pp. e11–e14, 2018.
[2] J. Piret and G. Boivin, "Pandemics throughout history," *Frontiers in Microbiology*, vol. 11, Article ID 631736, 2020.
[3] P. Singh, "Surface plasmon resonance: a boon for viral diagnostics," *Reference Module in Life Sciences*, 2017.
[4] X. D. Hoa, A. Kirk, and M. Tabrizian, "Towards integrated and sensitive surface plasmon resonance biosensors: a review of recent progress," *Biosensors and Bioelectronics*, vol. 23, no. 2, pp. 151–160, 2007.
[5] A. Kausaite, M. van Dijk, J. Castrop et al., "Surface plasmon resonance label-free monitoring of antibody antigen interactions in real time," *Biochemistry and Molecular Biology Education*, vol. 35, no. 1, pp. 57–63, 2007.
[6] J. Homola, "Surface plasmon resonance sensors for detection of chemical and biological species," *Chemical Reviews*, vol. 108, no. 2, pp. 462–493, 2008.
[7] L. Guo, J. A. Jackman, H.-H. Yang, P. Chen, N.-J. Cho, and D.-H. Kim, "Strategies for enhancing the sensitivity of plasmonic nanosensors," *Nano Today*, vol. 10, no. 2, pp. 213–239, 2015.
[8] H. Shi, T. Xia, A. E. Nel, and J. I. Yeh, *Part II: Coordinated Biosensors–Development of Enhanced Nanobiosensors for Biological and Medical Applications*, Future Medicine, Albert Place, London, UK, 2007.
[9] T. Riedel, C. Rodriguez-Emmenegger, A. De los Santos Pereira et al., "Diagnosis of Epstein–Barr virus infection in clinical serum samples by an SPR biosensor assay," *Biosensors and Bioelectronics*, vol. 55, pp. 278–284, 2014.
[10] C. Situ, M. H. Mooney, C. T. Elliott, and J. Buijs, "Advances in surface plasmon resonance biosensor technology towards high-throughput, food-safety analysis," *TrAC, Trends in Analytical Chemistry*, vol. 29, no. 11, pp. 1305–1315, 2010.
[11] H. K. Hunt and A. M. Armani, "Label-free biological and chemical sensors," *Nanoscale*, vol. 2, no. 9, pp. 1544–1559, 2010.
[12] P. Damborský, J. Švitel, and J. Katrlík, "Optical biosensors," *Essays in Biochemistry*, vol. 60, no. 1, pp. 91–100, 2016.
[13] P. Jahanshahi, Q. Wei, Z. Jie, M. Ghomeishi, S. D. Sekaran, and F. R. Mahamd Adikan, "Kinetic analysis of IgM monoclonal antibodies for determination of dengue sample

concentration using SPR technique," *Bioengineered*, vol. 8, no. 3, pp. 239–247, 2017.

[14] B. A. Prabowo, R. Y. Wang, M. K. Secario et al., "Rapid detection and quantification of Enterovirus 71 by a portable surface plasmon resonance biosensor," *Biosensors and Bioelectronics*, vol. 92, pp. 186–191, 2017.

[15] H. G. Franquelim, A. S. Veiga, G. Weissmüller, N. C. Santos, and M. A. Castanho, "Unravelling the molecular basis of the selectivity of the HIV-1 fusion inhibitor sifuvirtide towards phosphatidylcholine-rich rigid membranes," *Biochimica et Biophysica Acta (BBA)- Biomembranes*, vol. 1798, no. 6, pp. 1234–1243, 2010.

[16] M. H. Dietrich, K. M. Ogden, S. P. Katen et al., "Structural insights into reovirus σ1 interactions with two neutralizing antibodies," *Journal of Virology*, vol. 91, pp. 016211–e1716, 2017.

[17] R. H. Ritchie, "Plasma losses by fast electrons in thin films," *Physical Review*, vol. 106, no. 5, pp. 874–881, 1957.

[18] R. W. Wood, "XLII. On a remarkable case of uneven distribution of light in a diffraction grating spectrum," *The London, Edinburgh and Dublin Philosophical Magazine and Journal of Science*, vol. 4, no. 21, pp. 396–402, 1902.

[19] A. Otto, "Excitation of nonradiative surface plasma waves in silver by the method of frustrated total reflection," *Zeitschrift für Physik A Hadrons and nuclei*, vol. 216, no. 4, pp. 398–410, 1968.

[20] E. Kretschmann and H. Raether, "Notizen: radiative decay of non radiative surface plasmons excited by light," *Zeitschrift für Naturforschung A*, vol. 23, no. 12, pp. 2135-2136, 1968.

[21] E. Kretschmann, "Die bestimmung optischer konstanten von metallen durch anregung von oberflächenplasmaschwingungen," *Zeitschrift für Physik A Hadrons and nuclei*, vol. 241, no. 4, pp. 313–324, 1971.

[22] B. Liedberg, C. Nylander, and I. Lunström, "Surface plasmon resonance for gas detection and biosensing," *Sensors and Actuators*, vol. 4, pp. 299–304, 1983.

[23] M. Malmqvist, "BIACORE: an affinity biosensor system for characterization of biomolecular interactions," *Biochemical Society Transactions*, vol. 27, no. 2, pp. 335–340, 1999.

[24] R. L. Rich and D. G. Myszka, "Spying on HIV with SPR," *Trends in Microbiology*, vol. 11, no. 3, pp. 124–133, 2003.

[25] R. B. Schasfoort, J. van Weperen, M. van Amsterdam et al., "Presence and strength of binding of IgM, IgG and IgA antibodies against SARS-CoV-2 during CoViD-19 infection," *Biosensors and Bioelectronics*, vol. 183, Article ID 113165, 2021.

[26] F. Wu, J. Singh, P. A. Thomas et al., "Ultrasensitive and rapid detection of malaria using graphene-enhanced surface plasmon resonance," *2D Materials*, vol. 7, no. 4, Article ID 045019, 2020.

[27] C. T. Chou Chao, Y. F. Chou Chau, and H.-P. Chiang, "Highly sensitive metal-insulator-metal plasmonic refractive index sensor with a centrally coupled nanoring containing defects," *Journal of Physics D: Applied Physics*, vol. 54, no. 11, Article ID 115301, 2021.

[28] S. Zubaidah binti Haji Jumat, C. T. Chou Chao, Y. F. Chou Chau et al., "Plasmonic refractive index sensor based on the combination of rectangular and circular resonators including baffles," *Chinese Journal of Physics*, vol. 71, pp. 286–299, 2021.

[29] Y. F. Chou Chau, "Mid-infrared sensing properties of a plasmonic metal–insulator–metal waveguide with a single stub including defects," *Journal of Physics D: Applied Physics*, vol. 53, no. 11, Article ID 115401, 2020.

[30] C.-T. C. Chao, M. R. R. Kooh, C. M. Lim, R. Thotagamuge, A. H. Mahadi, and Y.-F. C. Chau, "Visible-range multiple-channel metal-shell rod-shaped narrowband plasmonic metamaterial absorber for refractive index and temperature sensing," *Micromachines*, vol. 14, no. 2, p. 340, 2023.

[31] Y.-F. C. Chau, C. T. C. Chao, H. J. Huang et al., "Strong and tunable plasmonic field coupling and enhancement generating from the protruded metal nanorods and dielectric cores," *Results in Physics*, vol. 13, Article ID 102290, 2019.

[32] Y. F. Chou Chau, J.-C. Jiang, C. T. Chou Chao, H.-P. Chiang, and C. M. Lim, "Manipulating near field enhancement and optical spectrum in a pair-array of the cavity resonance based plasmonic nanoantennas," *Journal of Physics D: Applied Physics*, vol. 49, no. 47, Article ID 475102, 2016.

[33] I. Choi and Y. Choi, "Plasmonic nanosensors: review and prospect," *IEEE Journal of Selected Topics in Quantum Electronics*, vol. 18, no. 3, pp. 1110–1121, 2012.

[34] M. A. Taylor and W. P. Bowen, "Quantum metrology and its application in biology," *Physics Reports*, vol. 615, pp. 1–59, 2016.

[35] V. Giovannetti, S. Lloyd, and L. Maccone, "Quantum-enhanced measurements: beating the standard quantum limit," *Science*, vol. 306, no. 5700, pp. 1330–1336, 2004.

[36] W. Fan, B. J. Lawrie, and R. C. Pooser, "Quantum plasmonic sensing," *Physical Review A*, vol. 92, no. 5, Article ID 053812, 2015.

[37] R. C. Pooser and B. Lawrie, "Plasmonic trace sensing below the photon shot noise limit," *ACS Photonics*, vol. 3, no. 1, pp. 8–13, 2016.

[38] C. Lee, F. Dieleman, J. Lee, C. Rockstuhl, S. A. Maier, and M. Tame, "Quantum plasmonic sensing: beyond the shot-noise and diffraction limit," *ACS Photonics*, vol. 3, no. 6, pp. 992–999, 2016.

[39] J.-S. Lee, T. Huynh, S.-Y. Lee et al., "Quantum noise reduction in intensity-sensitive surface-plasmon-resonance sensors," *Physical Review A*, vol. 96, no. 3, Article ID 033833, 2017.

[40] K. T. Mpofu, *Quantum plasmonic sensing with application to hiv research*, Ph.D. thesis, 2020, https://researchspace.ukzn.ac.za/bitstream/handle/10413/19509/Mpofu_Kelvin_Tafadzwa_2020.pdf?sequence=1.

[41] S. A. Maier, *Plasmonics: Fundamentals and Applications*, Springer, Berlin, Germany, 2007.

[42] S. Kawata, M. Ohtsu, and M. Irie, *Near-field Optics and Surface Plasmon Polaritons*, Springer Science and Business Media, Berlin, Germany, 2001.

[43] V. Naresh and N. Lee, "A review on biosensors and recent development of nanostructured materials-enabled biosensors," *Sensors*, vol. 21, no. 4, p. 1109, 2021.

[44] W. Yang, Y.-F. Chou Chau, and S.-C. Jheng, "Analysis of transmittance properties of surface plasmon modes on periodic solid/outline bowtie nanoantenna arrays," *Physics of Plasmas*, vol. 20, no. 6, 2013.

[45] L. Shen, T.-J. Yang, and Y.-F. Chau, "50/50 beam splitter using a one-dimensional metal photonic crystal with parabolalike dispersion," *Applied Physics Letters*, vol. 90, no. 25, 2007.

[46] Y.-F. Chau, Y.-J. Lin, and D. P. Tsai, "Enhanced surface plasmon resonance based on the silver nanoshells connected by the nanobars," *Optics Express*, vol. 18, no. 4, pp. 3510–3518, 2010.

[47] C.-T. Lin, M.-N. Chang, H. J. Huang et al., "Rapid fabrication of three-dimensional gold dendritic nanoforests for visible light-enhanced methanol oxidation," *Electrochimica Acta*, vol. 192, pp. 15–21, 2016.

[48] S. Szunerits and R. Boukherroub, "Sensing using localised surface plasmon resonance sensors," *Chemical Communications*, vol. 48, no. 72, pp. 8999–9010, 2012.

[49] K. L. Kelly, E. Coronado, L. L. Zhao, and G. C. Schatz, "The optical properties of metal nanoparticles: the influence of size, shape, and dielectric environment," *The Journal of Physical Chemistry B*, vol. 107, 2003.

[50] A. Cusano, A. Iadicicco, P. Pilla et al., "Mode transition in high refractive index coated long period gratings," *Optics Express*, vol. 14, no. 1, pp. 19–34, 2006.

[51] E. Voges, *Integrated Optics: Physics and Applications*, Springer, Berlin, Germany, 1983.

[52] J. Homola, I. Koudela, and S. S. Yee, "Surface plasmon resonance sensors based on diffraction gratings and prism couplers: sensitivity comparison," *Sensors and Actuators B: Chemical*, vol. 54, no. 1-2, pp. 16–24, 1999.

[53] S. Joseph, S. Sarkar, and J. Joseph, "Grating-coupled surface plasmon-polariton sensing at a flat metal–analyte interface in a hybrid-configuration," *ACS Applied Materials and Interfaces*, vol. 12, no. 41, pp. 46519–46529, 2020.

[54] S. Park, G. Lee, S. H. Song, C. H. Oh, and P. S. Kim, "Resonant coupling of surface plasmons to radiation modes by use of dielectric gratings," *Optics Letters*, vol. 28, no. 20, pp. 1870–1872, 2003.

[55] A. K. Sharma, R. Jha, and B. Gupta, "Fiber-optic sensors based on surface plasmon resonance: a comprehensive review," *IEEE Sensors Journal*, vol. 7, no. 8, pp. 1118–1129, 2007.

[56] W. Ding, S. Andrews, and S. Maier, "Internal excitation and superfocusing of surface plasmon polaritons on a silver-coated optical fiber tip," *Physical Review A*, vol. 75, no. 6, Article ID 063822, 2007.

[57] G. Liang, Z. Luo, K. Liu, Y. Wang, J. Dai, and Y. Duan, "Fiber optic surface plasmon resonance–based biosensor technique: fabrication, advancement, and application," *Critical Reviews in Analytical Chemistry*, vol. 46, no. 3, pp. 213–223, 2016.

[58] B. Špačková, M. Piliarik, P. Kvasnička, C. Themistos, M. Rajarajan, and J. Homola, "Novel concept of multi-channel fiber optic surface plasmon resonance sensor," *Sensors and Actuators B: Chemical*, vol. 139, no. 1, pp. 199–203, 2009.

[59] R. Kiselev, I. W. Schie, S. Aškrabić, C. Krafft, and J. Popp, "Design and first applications of a flexible Raman microspectroscopic system for biological imaging," *Biomedical Spectroscopy and Imaging*, vol. 5, no. 2, pp. 115–127, 2016.

[60] J.-S. Lee, S.-J. Yoon, H. Rah et al., "Quantum plasmonic sensing using single photons," *Optics express*, vol. 26, 2018.

[61] K. Mpofu, C. Lee, G. Maguire, H. Kruger, and M. Tame, "Measuring kinetic parameters using quantum plasmonic sensing," *Physical Review A*, vol. 105, no. 3, Article ID 032619, 2022.

[62] G. J. Wegner, H. J. Lee, G. Marriott, and R. M. Corn, "Fabrication of histidine-tagged fusion protein arrays for surface plasmon resonance imaging studies of protein- protein and protein- DNA interactions," *Analytical Chemistry*, vol. 75, no. 18, pp. 4740–4746, 2003.

[63] C. Xiao, *Super Optical Biosensors*, IOP Publishing, Bristol, United Kingdom, 2019.

[64] S. Hearty, P. J. Conroy, B. V. Ayyar, B. Byrne, and R. O'Kennedy, "Surface plasmon resonance for vaccine design and efficacy studies: recent applications and future trends," *Expert Review of Vaccines*, vol. 9, no. 6, pp. 645–664, 2010.

[65] M. Tame and C. Lee, "Plasmonics and sensing beyond classical limits," *Quantum Nanophotonic Materials, Devices, and Systems*, vol. 11091, pp. 21–30, 2019.

[66] K. Mpofu, C. Lee, G. Maguire, H. Kruger, and M. Tame, "Experimental measurement of kinetic parameters using quantum plasmonic sensing," *Journal of Applied Physics*, vol. 131, no. 8, Article ID 084402, 2022.

[67] J. N. Anker, W. P. Hall, O. Lyandres, N. C. Shah, J. Zhao, and R. P. Van Duyne, "Biosensing with plasmonic nanosensors," *Nature Materials*, vol. 7, no. 6, pp. 442–453, 2008.

[68] C. Gerry, P. Knight, and P. L. Knight, *Introductory Quantum Optics*, Cambridge University Press, Cambridge, United Kingdom, 2005.

[69] R. Loudon, *The Quantum Theory of Light*, OUP Oxford, Oxford, United Kingdom, 2000.

[70] L. Mandel, "Sub-Poissonian photon statistics in resonance fluorescence," *Optics Letters*, vol. 4, no. 7, pp. 205–207, 1979.

[71] R. J. Barlow, *Statistics: A Guide to the Use of Statistical Methods in the Physical Sciences*, John Wiley and Sons, Hoboken, NJ, USA, 1993.

[72] O. Pluchery, R. Vayron, and K.-M. Van, "Laboratory experiments for exploring the surface plasmon resonance," *European Journal of Physics*, vol. 32, no. 2, pp. 585–599, 2011.